Electronic Supplementary Information (ESI)

3D hierarchical porous N-doped carbon quantum dots/vanadium nitride hybrid microflowers as a superior electrode material toward high-performance asymmetric capacitive deionization

Jingxuan Zhao, [a] Zhibo Zhao, [a] Yang Sun, [a] Xiangdong Ma, [a] Meidan Ye, [*b] and Xiaoru Wen [*a]

[a] *College of Chemistry and Chemical Engineering, Inner Mongolia University, No. 235 College Road, Hohhot, 010021, China.*
[b] *Research Institute for Biomimetics and Soft Matter, Fujian Provincial Key Laboratory for Soft Functional Materials Research, Department of Physics, Xiamen University, No. 422 Siming South Road, Xiamen, 361005, China.*
[*] *Corresponding author:*
Dr. Xiaoru Wen; E-mail: xiaoru-wen@outlook.com
Dr. Meidan Ye; E-mail: mdye@xmu.edu.cn

EXPERIMENTS

Preparation of NCQDs

Herein, the NCQDs were synthesized by a traditional hydrothermal processing. Firstly, 720 mg of urea and 840 mg of citric acid were absolutely dissolved in 20 mL of distilled water, and the mixture was further stirred for 10 min at the room temperature. Then the solution was transferred to a 50 mL of Teflon-lined autoclave, and kept at 160 °C for 5 h.

Preparation of NCQDs/VN with different NCQDs dopant amount

For comparison, the NCQDs/VN hybrids with different NCQDs dopant amount were also fabricated. Typically, 0.1 g of VCl_3 was sufficiently dispersed in 25 mL of solution with NCQDs dopant varying from 5 to 25 mL, and then 4 mL of ammonia solution (25 wt.%) was slowly dropped into the above mixture. The obtained limpid solution was transferred into the autoclave of 50 mL followed by being heated at 200 °C for 24 h. Subsequently, the black precipitate was absolutely rinsed and further annealed at 600 °C under the NH_3 atmosphere similar to the pristine VN powder. The resultant samples were donated as NCQDs-5/VN, NCQDs-10/VN, NCQDs-20/VN (e.g. NCQDs/VN) and NCQDs-25/VN.

Material characterizations

X-ray photoelectron spectroscopy (XPS) measurements were firstly conducted to reveal the surface composition and chemical state in a VG Scientific ESCALAB Mark II spectrometer equipped with two ultrahigh vacuum (UHV) chambers, and all spectra were calibrated with the C-C peak of C1s orbitals (e.g., 284.6 eV). The X-ray diffraction (XRD) was performed with a Rigaku D/MAX-RB X-ray diffractometer by using Cu Kα (40 kV, 20 mA) radiation and a secondary beam graphite monochromator. The Raman spectra were recorded on an in-equipped with an optical microscope with the excitation of 514.5 nm line from an Ar^+ ion laser (Spectra Physics). The N_2 adsorption/desorption tests were performed on an ASAP 2020 Brunauer-Emmett-Teller (BET) analyser. Correspondingly, the specific surface area and pore volume were calculated with the BET method, and the pore size distribution was also estimated with desorption branches. In addition, the texture morphology and structure of NCQDs/VN and pristine VN powders were further observed by the field emission scanning electron microscopy (SEM, Hitachi S-4800), Energy Dispersive Spectrometer (EDS) and transmission electron microscopy (TEM, FEI Tecnai F20).

Electrochemical performance measurements

The powder electrodes were prepared by a traditional slurry-coating processing as mentioned previously.[1] Typically, the prepared active powder (e.g., NCQDs/VN or VN) of 10 mg, acetylene black and polytetrafluoroethylene (PTFE) binder with a weight ratio of 8:1:1 were ground effectively, which formed a uniform slurry. Then, the obtained mixture was further coated onto the widely used graphite paper substrate with a square (1 cm × 1 cm × 0.1 cm) film, and the resultant powder electrodes donated as NCQDs/VN or VN was constructed after being dried at 120 °C overnight.

The electrochemical performance of hierarchically porous NCQDs/VN hybrid and pristine VN powder electrodes were analyzed by CHI660E by measuring cyclic voltammetry (CV), electrochemical impedance spectroscopy (EIS), and galvanostatic charge/discharge (GC) plots. Here, the constructed active electrode, graphite sheet, and saturated calomel electrode acted as the working, counter and reference electrodes, respectively.

In detail, the CV measurements were performed on the CHI-660E, and the specific capacitance donated as the C_m was calculated.

$$C_m=Q/mv\triangle V \quad (S1)$$

where m was the active mass of 10 mg, $\triangle V$ was the range of chosen potential, v was the running scan rate, and Q was the integrated curve area.

The GC measurements were conducted using an automatic LAND battery test instrument (Land CT2001A) to evaluate capacitive property and cycling performance of as-prepared electrodes. Moreover, the Coulombic efficiency (η, %) was obtained by the ratio between t_d and t_c as follow. The t_c was the charging time, and the t_d was the discharging time.[3]

$$\eta=t_d/t_c\times100 \quad (S2)$$

The EIS measurements were also carried out on the CHI-660E in a frequency window from 10 mHz to 100 kHz, and the amplitude of alternating voltage was 5 mV around the equilibrium potential of 0 V.

Supplementary figures

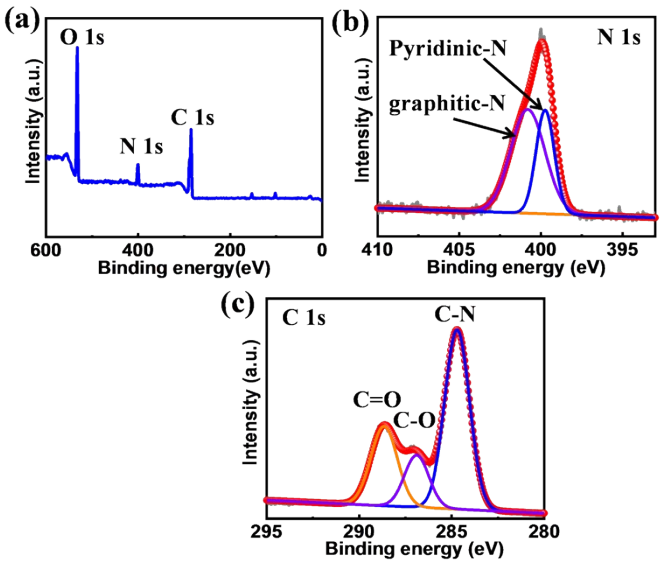

Fig. S1 (a) Full range XPS spectrum and (b-c) high-resolution XPS spectra (N1s and C1s) of the as-prepared NCQDs powders.

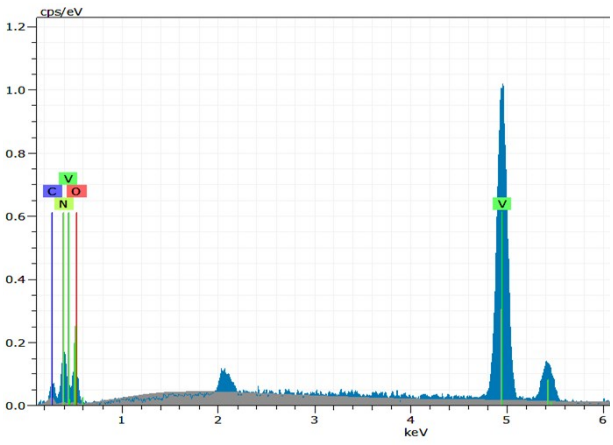

Fig. S2 EDS element mapping of V, N, C and O of the hierarchically porous NCQDs/VN hybrid.

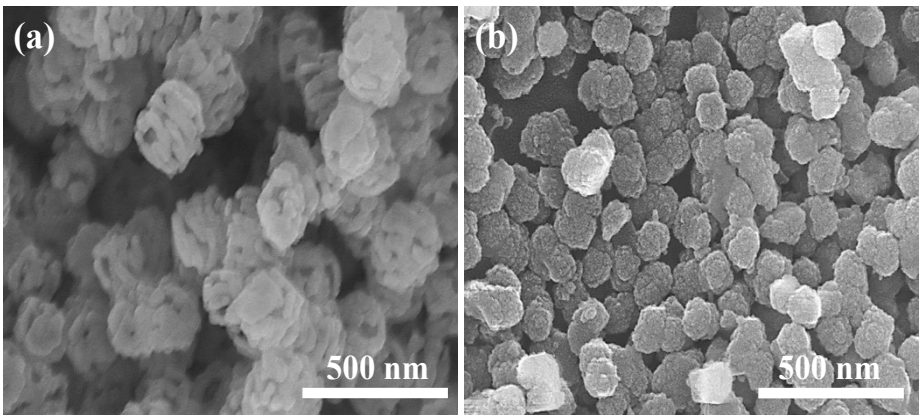

Fig. S3 SEM images of the as-prepared pristine VN (a) and NCQDs (b).

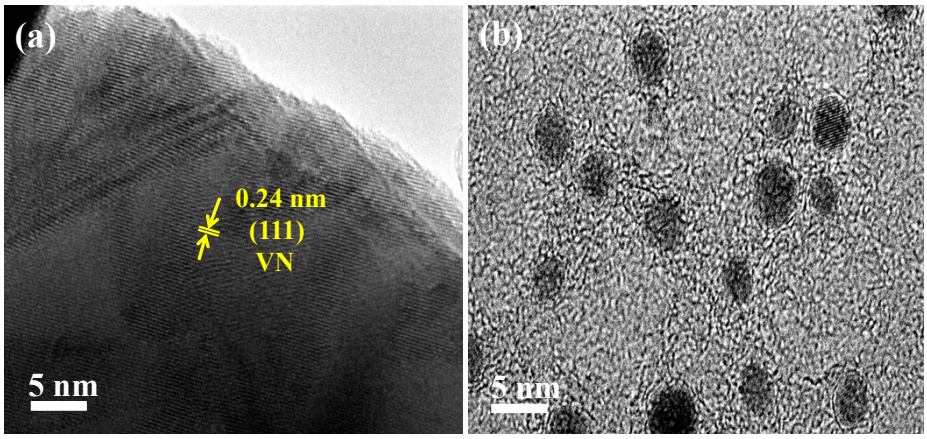

Fig. S4 TEM images of the as-prepared pristine VN (a) and NCQDs (b).

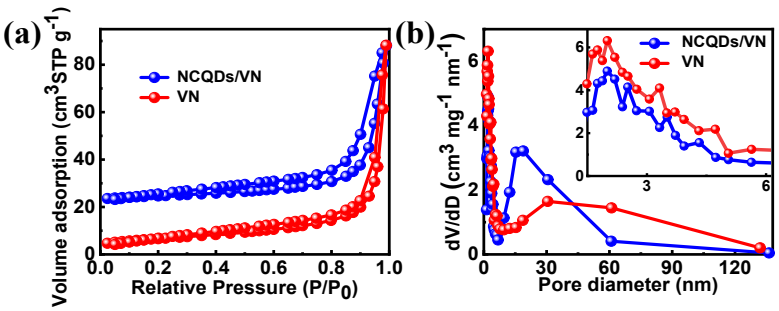

Fig. S5 (a) N_2 adsorption/desorption isotherms, and (b) pore size distribution plots of the as-prepared hierarchically porous NCQDs/VN hybrid and pristine VN.

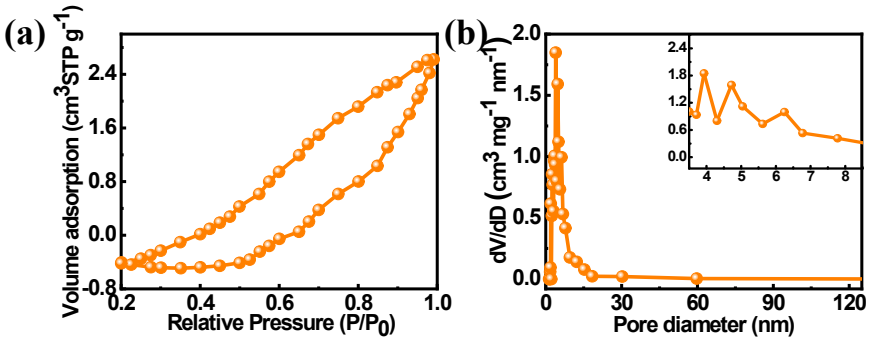

Fig. S6 (a) N_2 adsorption/desorption isotherms and (b) pore size distribution plots of the as-prepared NCQDs powder.

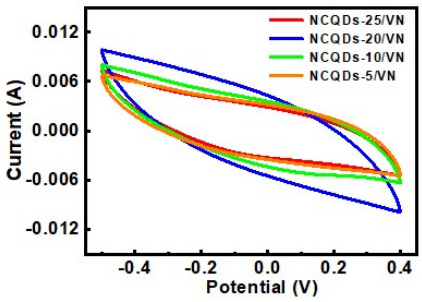

Fig. S7 CVs of the as-prepared NCQDs/VN electrode with the different amount of NCQDs dopant at a scan rate of 10 mV/s.

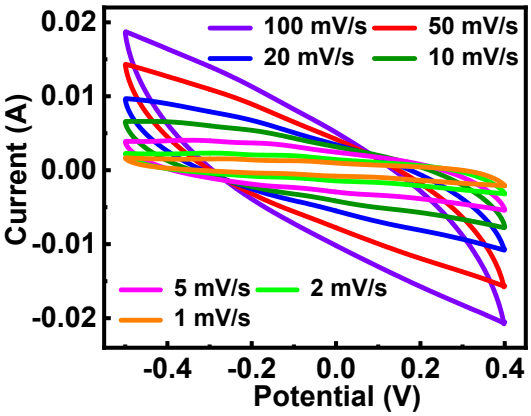

Fig. S8 CVs of the as-prepared NCQDs powder electrode at scan rates from 1 to 100 mV/s.

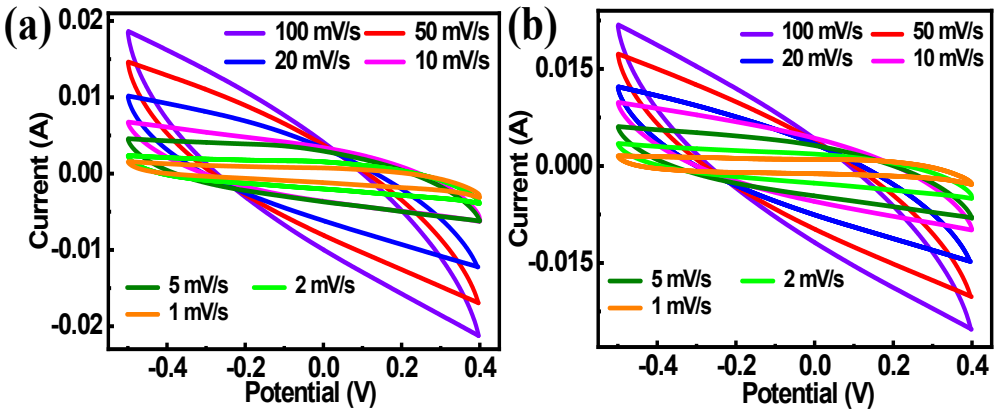

Fig. S9 CVs of the as-prepared NCQDs/VN (a) and VN (b) powder electrodes at scan rates from 1 to 100 mV/s.

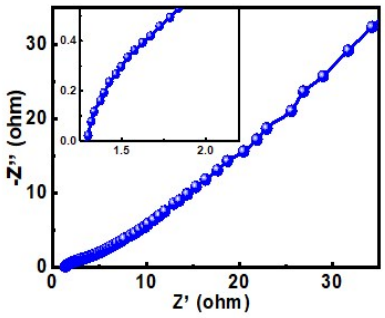

Fig. S10 Nyquist impedance curve of the as-prepared NCQDs powder electrode in a NaCl solution of 1 M.

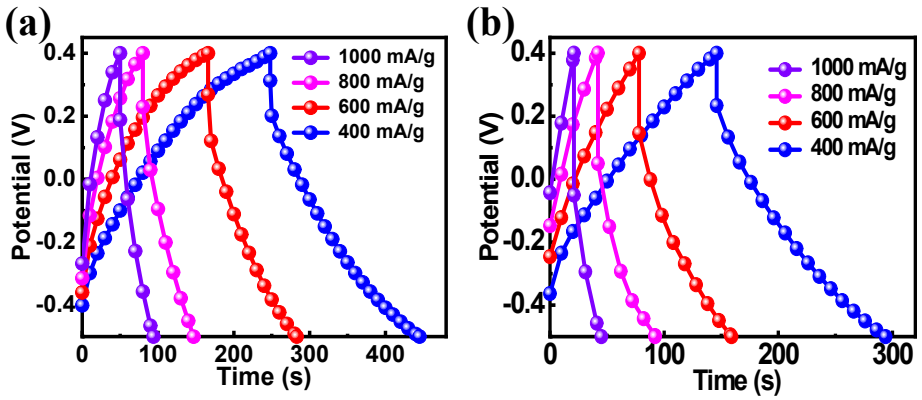

Fig. S11 GC plots of the as-prepared NCQDs/VN (a) and VN (b) powder electrodes at current loads from 400 to 1000 mA/g.

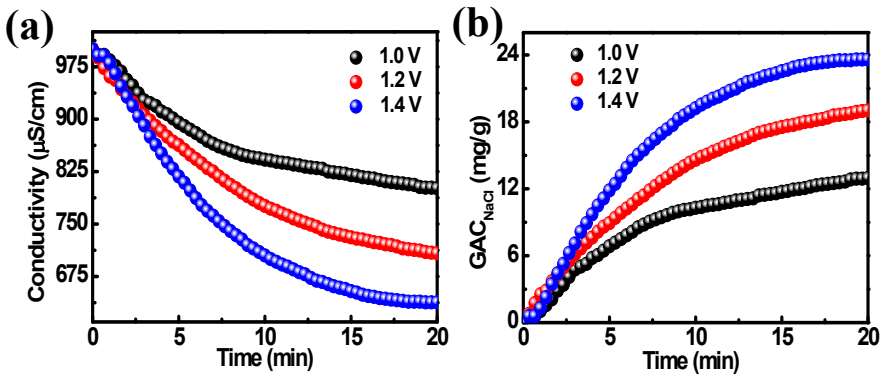

Fig. S12 The CDI performance of as-prepared NCQDs/VN powder electrodes: (a) comparative solution conductivity and (b) dynamic GAC_{NaCl} vs. running time upon different applied voltages from 1.0 to 1.4 V.

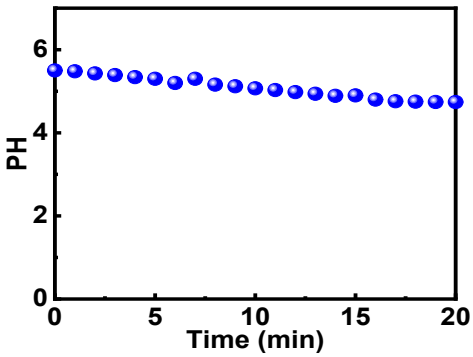

Fig. S13 Transient PH value vs. running time of the NCQDs/VN hybrid electrode-based CDI cell.

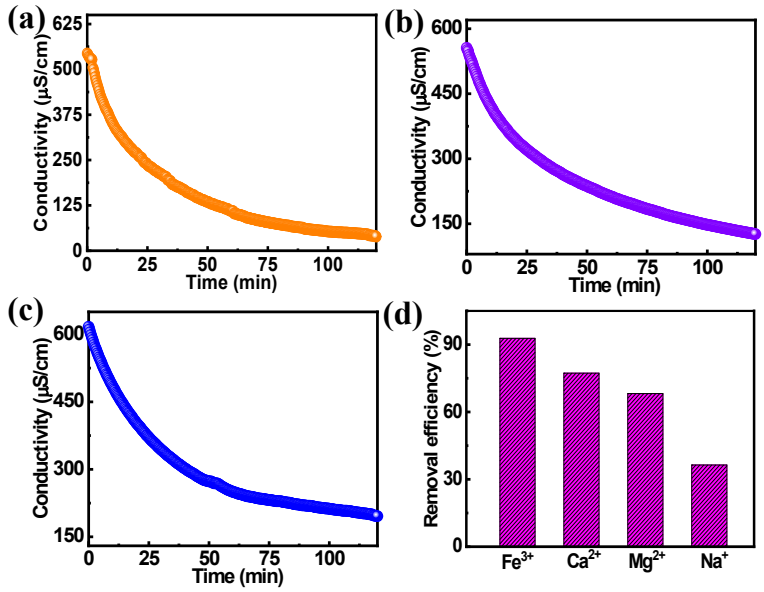

Fig. S14 Transient solution conductivity vs. running time in different metal cation solution: (a) $FeCl_3$, (b) $CaCl_2$ and (c) $MgCl_2$, and (d) corresponding removal efficiencies of NCQDs/VN hybrid electrode-based CDI cell.

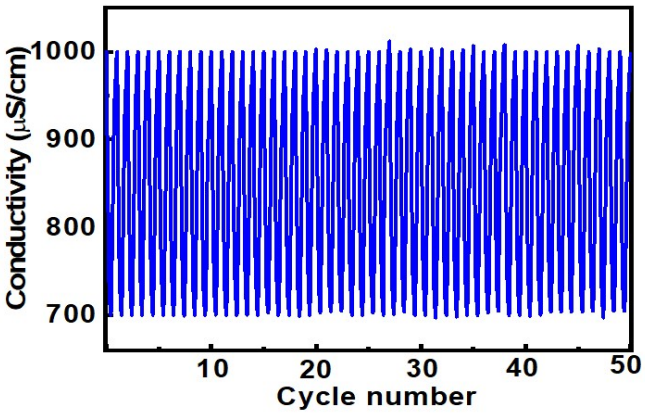

Fig. S15 Regenerration profiles of the NCQDs/VN hybrid electrode during the overall cycling of 50.

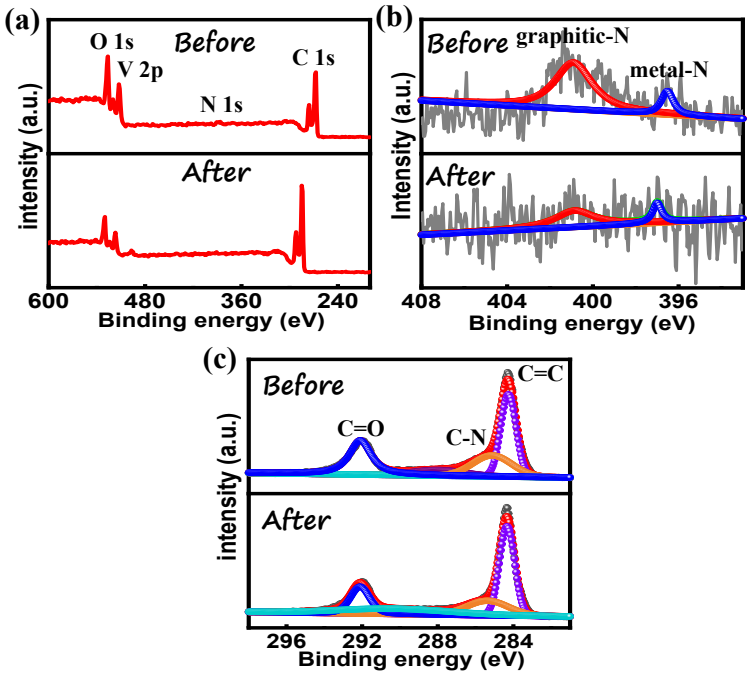

Fig. S16 (a) Full range XPS spectrum and (b-c) high-resolution XPS spectra (N1s and C1s) of the NCQDs/VN hybrid electrode before and after the continiuous CDI cycling.

Supplementary Tables

Table S1 Elemental distribution of the hierarchically porous NCQDs/VN hybrid (atomic content %).

Element	V	N	O	C	Total
Atom (at. %)	33.10	29.99	24.00	12.91	100

Table S2 Surface texture properties of the pristine VN, NCQDs and hierarchically porous NCQDs/VN hybrid.

	S_{BET} (m^2/g)	V_{BJH} (cm^3/g)	D_{Pore} (nm)
NCQDs/VN	36.57	0.14	2.00
VN	32.49	0.11	2.00
NCQDs	4.91	0.01	3.93

Table S3 Comparative results on adsorption capacities among reported different nanomaterials.

Samples	NaCl concentration (mg/L)	Voltage (V)	Adsorption capacity (mg/g)	Ref.
Ce-MoS_2 Nanosheets	400	1.2	8.81	4
Ia3d-CS-2	100	1.2	1.31	5
TiS_2-10CNT	600	0.8	14.5	6
CeO_2@GNFs	48	1.4	7.2	7
MoS_2/PDA	500	1.2	14.80	8
LDH-AC	500	1.2	13.9	9
NP-HPCNs	250	1.2	10.3	10
NCQDs/VN	500	1.2	19.28	This work

References

1. X. R. Wen, M. Q. Zhao, Z. B. Zhao, X. D. Ma and M. D. Ye, Hierarchical and self-supported vanadium disulfide microstructures@graphite paper: an advanced electrode for efficient and durable asymmetric capacitive deionization, *ACS Sustainable Chem. Eng.,* 2020**, 8,** 7335-7342.
2. J. Zhang, T. T. Yan, J. H. Fang, J. J. Shen, L. Y. Shi and D. S. Zhang, Enhanced capacitive deionization of saline water using N-doped rod-like porous carbon derived from dual-ligand metal-organic frameworks, *Environ. Sci.: Nano,* 2020**, 7,** 926-937.
3. M. Li and H. G. Park, Pseudocapacitive coating for effective capacitive deionization, *ACS appl. Mater. Interfaces,* 2018**, 10,** 2442-2450.
4. F. Xing, T. Li, J. Y. Li, H. R. Zhu, N. Wang and X. Cao, Chemically exfoliated MoS_2 for capacitive deionization of saline water, *Nano Energy,* 2017, **31,** 590-595.
5. C. Cao, X. Wu, Y. Zheng and Y. Chen, Three-dimensional cubic ordered mesoporous carbon with chitosan for capacitive deionization disinfection of water, *Environ. Sci. pollut. R.,* 2020**, 27,** 15001-15010.
6. P. Srimuk, J. Lee, A. Tolosa, C. Kim, M. Aslan and V. Presser,Titanium disulfide: a promising low-dimensional electrode material for sodium ion intercalation for seawater desalination, *Chem. Mater.,* 2017, **29,** 9964-9973
7. A. Yousef, A. M. Al-Enizi, I. M. A. Mohamed, M. M. El-Halwany, M. Ubaidullah and R. M. Brooks, Synthesis and characterization of CeO_2/rGO nanoflakes as electrode material for capacitive deionization technology, *Ceram. Int.,* 2020, **46,** 15034-15043.
8. Q. M. Wang, F. F. Jia, S. X. Song and Y. M. Li, Hydrophilic MoS_2/polydopamine (PDA) nanocomposites as the electrode for enhanced capacitive deionization, *Sep. Purif. Technol.,* 2020, **236,** 116298-116331.
9. J. Lee, S. Kim, N. Kim, C. Kim and J. Yoon, Enhancing the desalination performance of capacitive deionization using a layered double hydroxide coated activated carbon electrode, *Appl. Sci.,* 2020**, 10,** 403-412.
10. S. L. Huo, Y. B. Zhao, M. Z. Zong, B. L. Liang, X. L. Zhang, I. U. Khan, X. Song, and K. X. Li, Boosting supercapacitor and capacitive deionization performance of hierarchically porous carbon by polar surface and structural engineering, *J. Mater. Chem. A,* 2020**, 8,** 2505-2517.